POLITECNICO MILANO 1863

Politecnico di Milano
Scuola di Ingegneria

MECHANICAL ENGINEERING: MECHATRONICS AND ROBOTICS

*Academic Year 2025/2026*

# Advanced Dynamics of Mechanical Systems

*Project Report*

**Authors:**

Caterina Brunetti
Alessia Cecchini
Federico Della Vittoria
Tareq El Kajjyouy

**June 2026**

# Finite Element Analysis of the 2026 Olympic Ski Jump

## 1.5 Introduction

The objective of our project work is to perform a Finite Element Analysis (FEA) of the structure shown in Figure 1.29, which represents a two-dimensional idealization of the ski jumping hill designed for the Milano–Cortina Winter Olympic Games in Predazzo. The sliding track consists of a straight segment followed by a curved portion modeled as a circular arc with a radius of 112 m. The track is supported by two steel lattice frameworks, which provide the overall stiffness and stability to the structure. The entire system is modeled as a planar frame and the geometric and material properties are reported in Figure 1.29.


Figure 1.28: Real structure

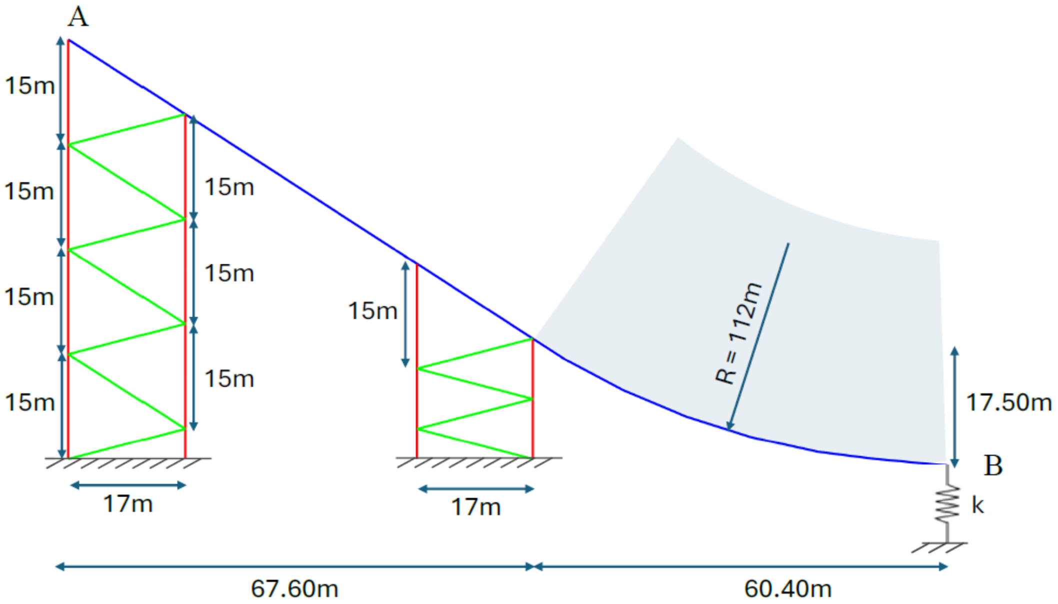


| | m[kg/m] | EA [N] | EJ[Nm²] |
|---|---|---|---|
| Red beams | 122 | 3.21E9 | 2E8 |
| Green beams | 80 | 1.74E9 | 4.8E7 |
| Blue beams | 400 | 2.5E9 | 4.0E9 |

Figure 1.29: Planar representation of the structure and material properties

The stiffness of the linear spring is assumed equal to $5 \cdot 10^7 N/m$ and the damping is defined according to the *proportional damping* assumption:
$[C] = \alpha[M] + \beta[K]$, with $\alpha = 0.1s^{-1}$ and $\beta = 2.0 \cdot 10^{-4}s$.

We are required to investigate the dynamic behavior of the structure and evaluate different Frequency Response Functions (FRFs) under various scenarios.

## 1.6 Definition of the FE model

The first task consists on defining the finite element model of the structure within the 0–6 Hz frequency range ($\Omega_{max} = 6Hz$), considering the safety factor as $\eta = 1.5$. Consequently, the length of each finite element, for each material considered, is determined according to the equation 1.18, derived from the theory of pinned–pinned beams:

$$L_{max} = \sqrt{\frac{\pi^2}{\eta\Omega_{max}}\sqrt{\frac{EJ}{m}}} \tag{1.18}$$

This criterion must be applied to ensure that the shape functions used to interpolate the displacement field between the nodes remain valid within the static regime. Therefore, it is necessary to satisfy the condition: $\Omega_{max} << \omega_1$. This assumption guarantees that each finite element is in the quasi-static region, allowing the shape functions to be employed under the hypothesis of static behavior at the element level. The resulting element length for each beam type, characterized by different materials, are summarized in the table below.

Table 1.5: $L_{max}$ value for each material

| Material | $L_{max}$ |
|---|---|
| Light green beam | 14.9m |
| Dark green beam | 11.6m |
| Blue beam | 23.5m |

Once the input file that contains all the geometric and material information is defined, the complete finite element model of the structure can be generated and plotted on MATLAB through the `loadstructure` and `dis_stru` functions, respectively, with all the nodes and elements according to the adopted FEM discretization.

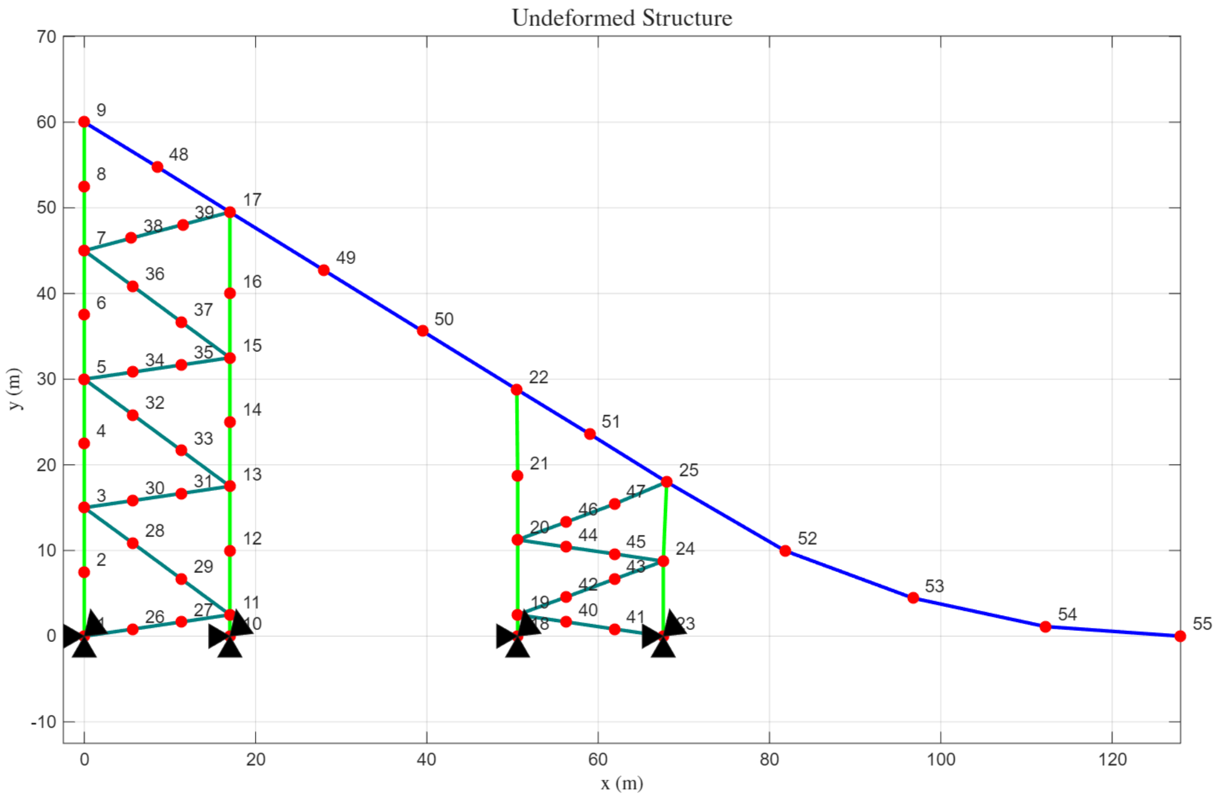


Figure 1.30: Structure's mesh

Table 1.6: Structural model properties

| Description | Value |
|---|---|
| Number of structure nodes | 55 |
| Number of structure d.o.f. | 153 |
| Number of materials | 3 |
| Number of beam FE | 65 |

## 1.7 Determination of the eigenfrequencies and the mode shapes

The next step consists on determining the eigenfrequencies and mode shapes of the ski jumping hill structure.

To evaluate the natural frequencies, it is necessary to compute the global mass and stiffness matrices of the entire structure. In this case, particular attention must be paid to the stiffness matrix, since the contribution of the spring element, modeled as a lumped parameter, must also be included.

The assembly of the final matrices is carried out in two stages.

Firstly, the `assem` function in MATLAB is employed, as it accounts for both the physical properties and the geometric characteristics of the structure. The elemental mass $[M]$ and stiffness $[K]$ matrices are obtained, initially in the local reference system and subsequently transformed into the global reference system according to the following relations:

$$[M_{k,GLOB}] = [\Lambda_k]^T [M_{k,LOC}][\Lambda_k]$$
$$[K_{k,GLOB}] = [\Lambda_k]^T [K_{k,LOC}][\Lambda_k]$$

The second step consists of adding the contribution of the lumped parameter element directly into the corresponding global matrices through the *idb* matrix, considering a vertical stiffness contribution of $5 \cdot 10^7 N/m$ applied at node 65.

Once the global mass $[M]$ and stiffness $[K]$ matrices have been assembled, the natural frequencies and mode shapes of the system can be determined by solving the following eigenvalue problem:

$$(\omega^2[I] - [M_{FF}]^{-1}[K_{FF}])X = 0 \tag{1.19}$$

Where the matrices $[M_{FF}]$ and $[K_{FF}]$ are the global mass and stiffness matrices that consider only the free DOFs and their interaction.

The eigenvalue problem can be solved using the MATLAB `eig` function, which returns a diagonal matrix containing the eigenvalues and a matrix whose columns correspond to the associated eigenvectors.

The eigenvectors are then ordered in ascending order according to the natural frequencies. Finally, by using the `diseg2` function and selecting an appropriate scale factor to enhance the visualization of the deformation shapes (equal to 10 in this case), it is possible to plot the mode shapes of the structure (Images 1.31, 1.32, 1.33 and 1.34).

The obtained eigenfrequencies values are reported in Table 1.7.

Table 1.7: Eigenfrequencies values

| **Mode** | $f$ |
|---|---|
| 1 | 1.57 Hz |
| 2 | 2.97 Hz |
| 3 | 4.91 Hz |
| 4 | 5.29 Hz |

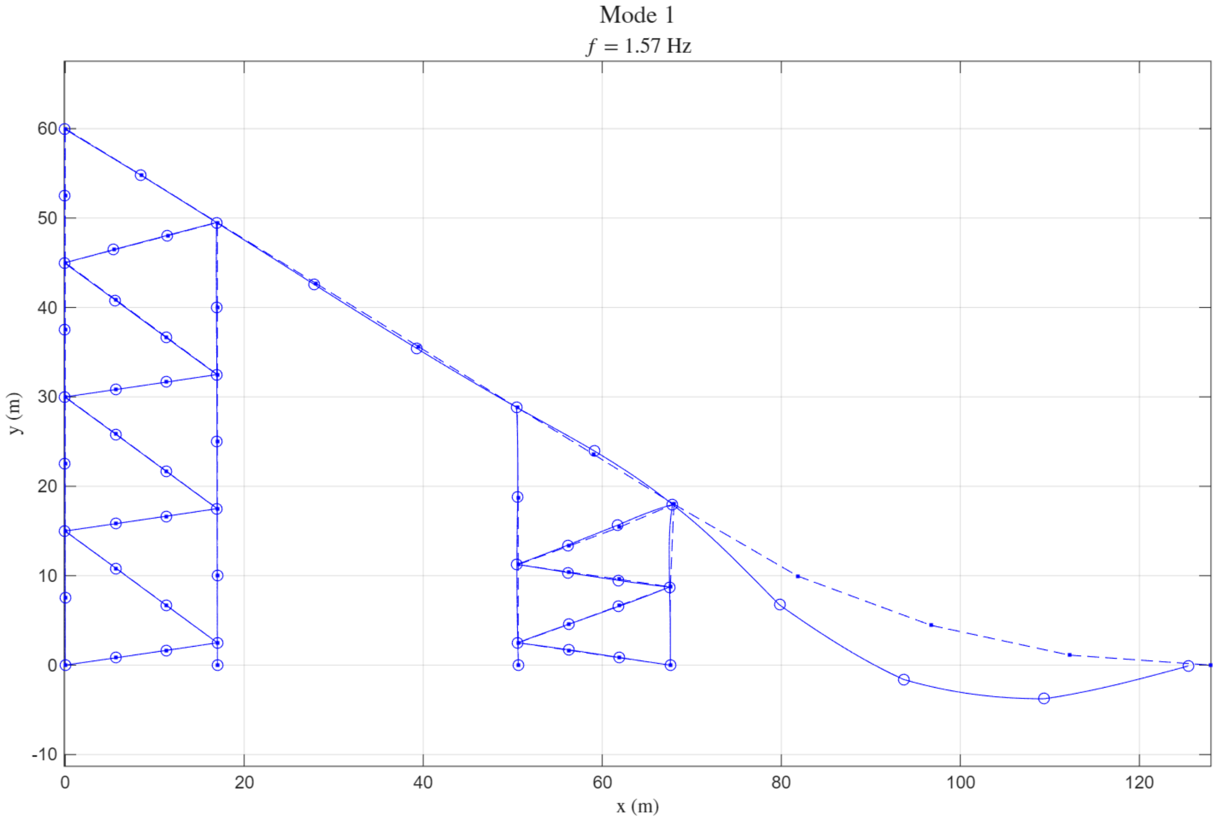


Figure 1.31: First mode shape

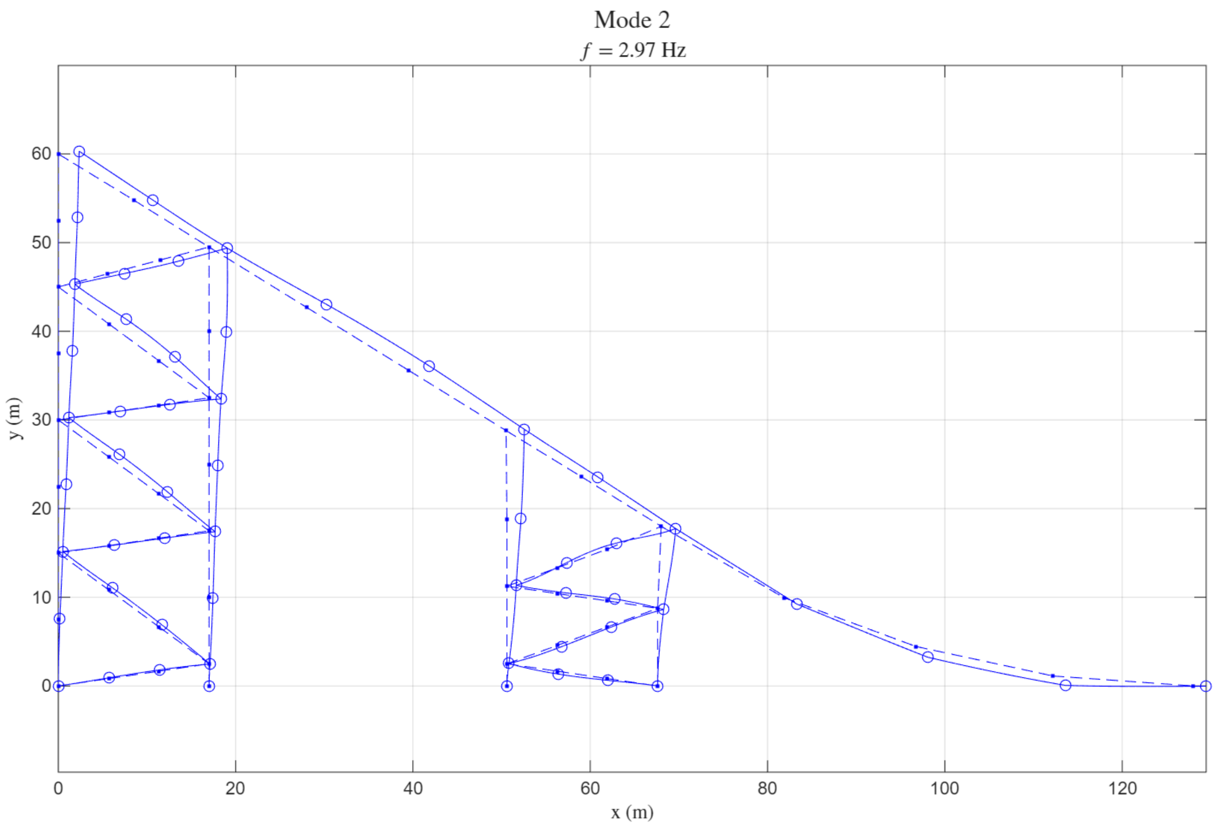


Figure 1.32: Second mode shape

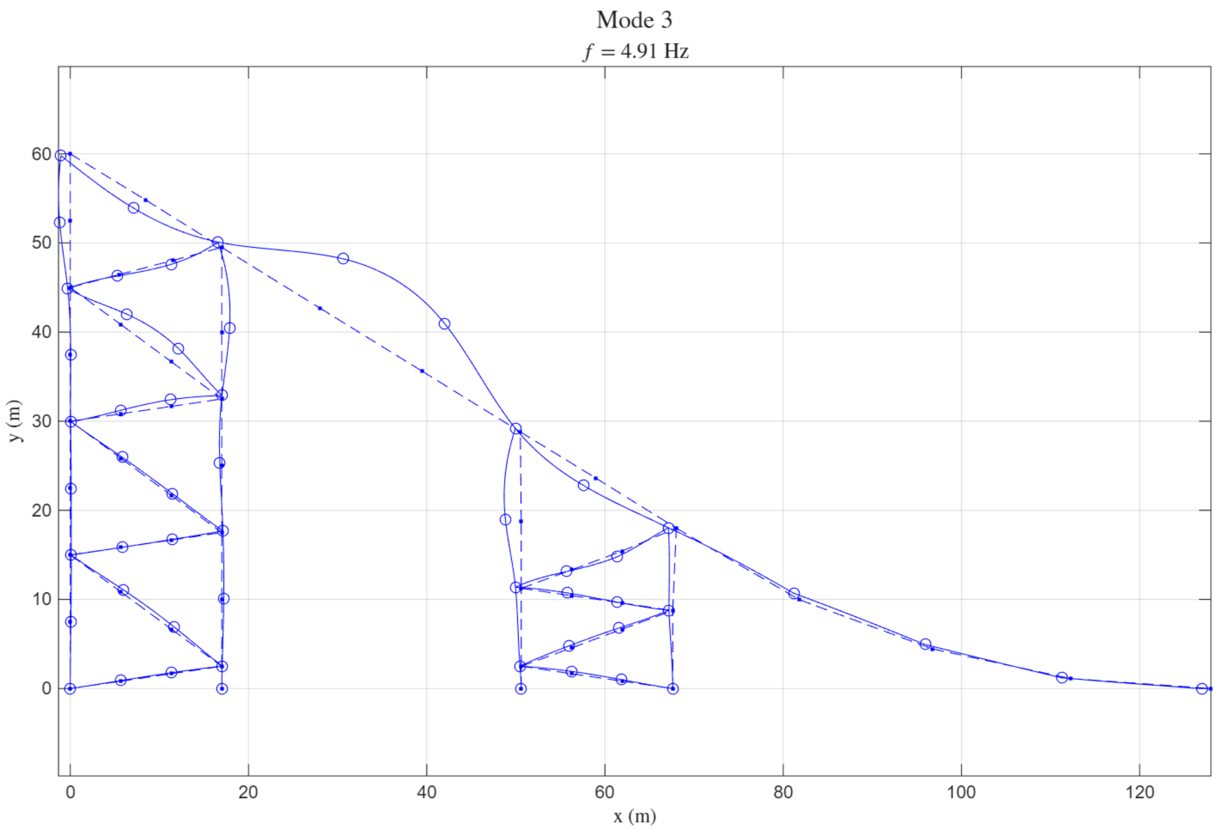


Figure 1.33: Third mode shape

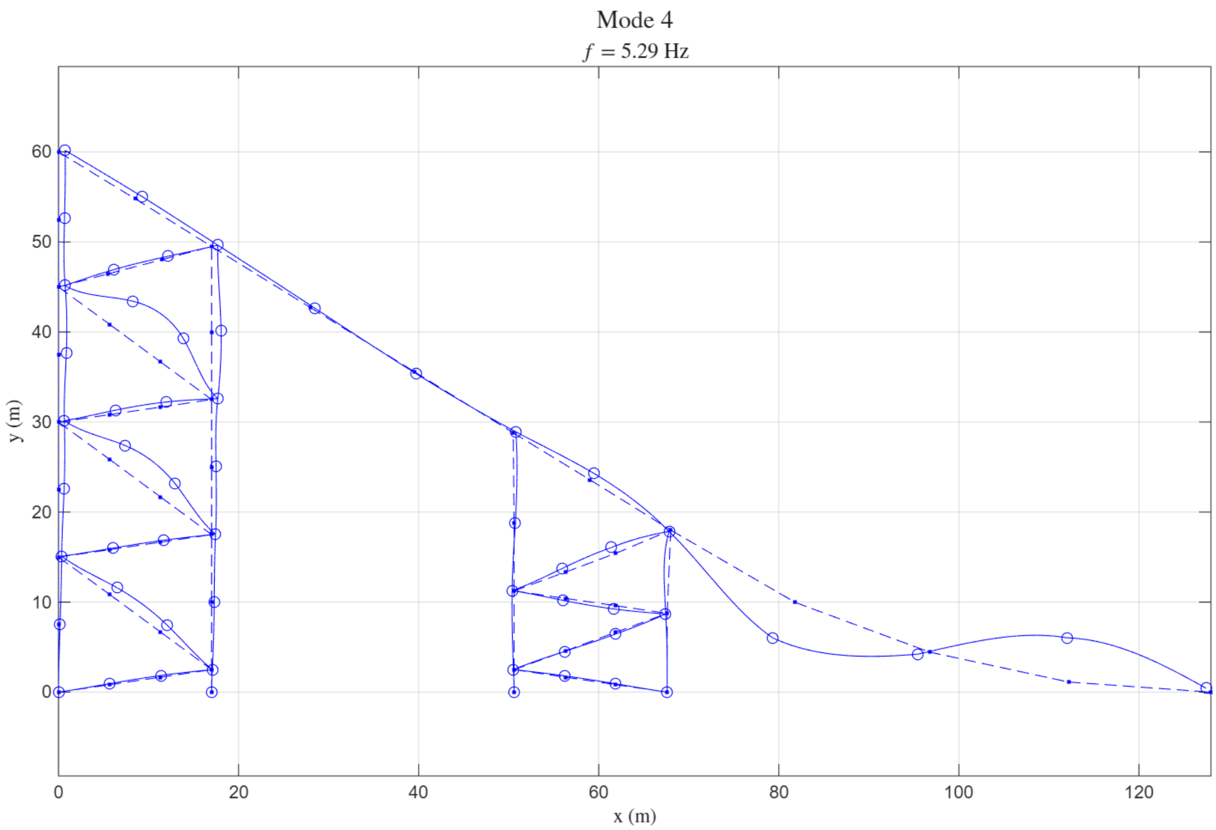


Figure 1.34: Fourth mode shape

## 1.8 FRFs: FEM model

The analysis now moves to the evaluation of the FRF of the system as forces are applied in different points of the structure.
Specifically, the first case requires to consider two scenarios: the horizontal response in point A and the vertical response in point B caused by an horizontal force applied in A in both cases. We can leverage on the Formula 1.20 to calculate $\mathbf{X_0}$:

$$\mathbf{F_0} = (-\Omega^2[M_{FF}] + i\Omega[C_{FF}] + [K_{FF}])\mathbf{X_0}\,, \tag{1.20}$$

In order to display the FRFs associated only to horizontal output in A and the vertical output in B, it was necessary to exploit the provided *idb* matrix.

The FRFs' plots reported below show a main difference: the first eigenfrequency (1.57 $Hz$) is almost not visible when looking at the FRF in point A (i.e. co-located FRF) (Figure 1.35), while showing a remarkable resonance for point B (Figure 1.36).

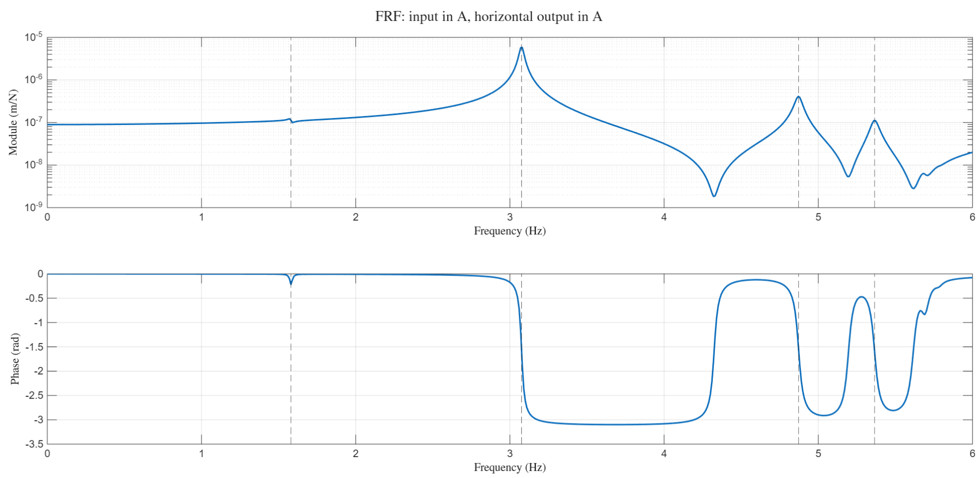


Figure 1.35: Input in A, horizontal output in A.

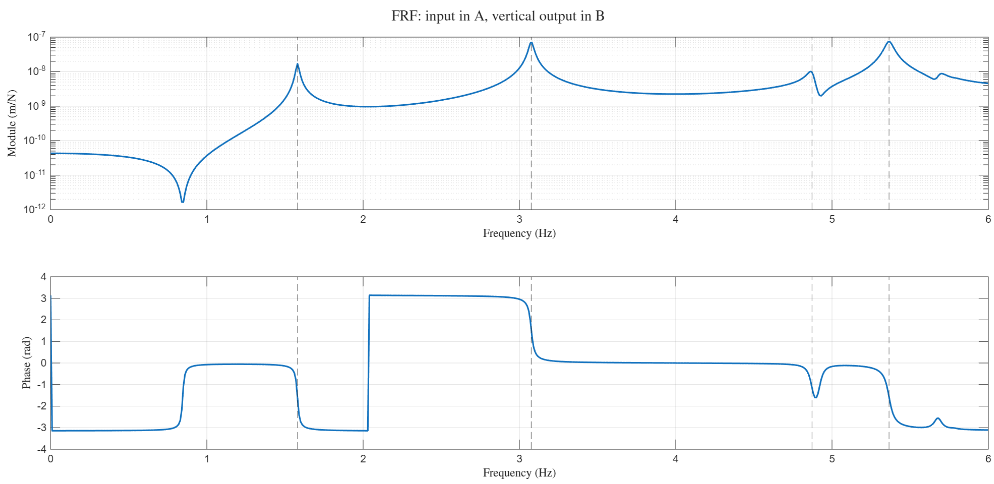


Figure 1.36: Input in A, vertical output in B.

The FRF exhibits a very small resonance peak for the first eigenfrequency. This behavior can be explained by examining the first vibration mode of the structure. In fact, by looking at the first mode shape, the point A has a almost null deformation in the horizontal direction, consequently, a very small resonance peak is in the FRF.

## 1.9 FRFs: Modal Approach

Inverting the input and the output position and orientation (vertical force applied in B, measure of the horizontal displacement in A), the FEM approach is here compared with the modal approach - focusing on the first two modes. In order to compute the modal result we define the modal mass and stiffness matrices as follows:

$$[M_q] = [\Phi]^T[M][\Phi] \tag{1.21}$$

$$[K_q] = [\Phi]^T[K][\Phi] \tag{1.22}$$

$$[C_q] = [\Phi]^T[C][\Phi] \tag{1.23}$$

The Figure 1.37 highlights how the modal approach is able to capture the considered eigenfrequencies, even though significant differences exist as looking at the phase diagram. As we can see, we have that the resonances of both FEM and modal representation are

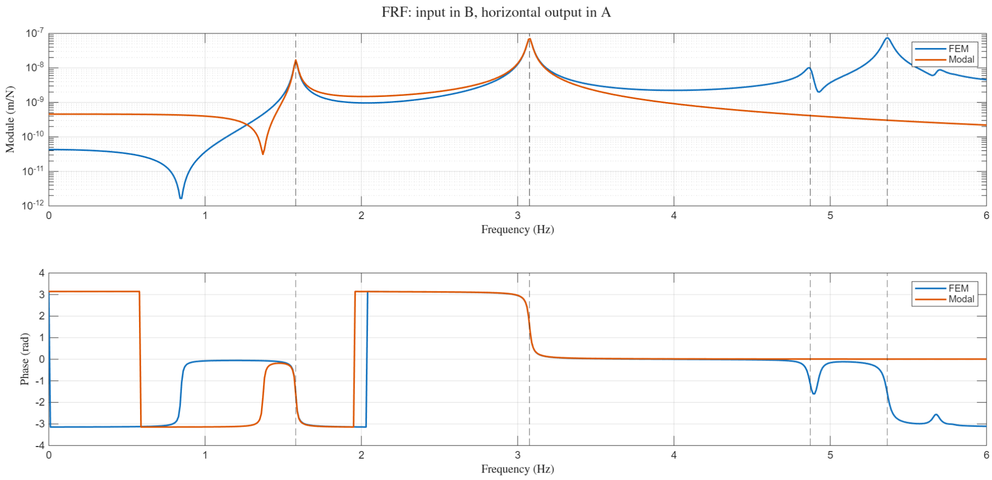


Figure 1.37: Input in B, horizontal output in A.

occurring at the same frequency index.

## 1.10 Static response of the system

Then, to account for a more realistic case, that is of snow presence over the ski jumping hill, we proceed with the consideration of the distributed load.
The first and main challenge is to properly represent the force. Initially, we define it in the local reference frame, then through the rotation matrix we move it to the global reference system and, finally, exploiting the extraction matrix, we can associate to it the loaded nodes (i.e. those corresponding to the sliding track).
In order to measure the maximum displacement, we evaluate all the distances of the displaced elements, and selected the maximum value, that corresponds to $0.174m$.

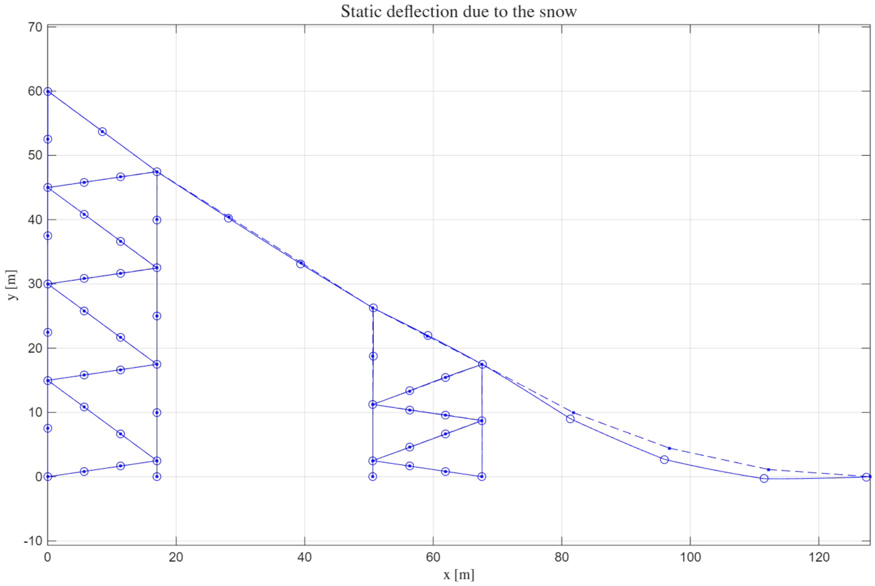


Figure 1.38: Static deflection due to the snow.

## 1.11 Vertical displacement of point B

In this chapter, we have modeled a skier who jumps from the ramp with a concentrated traveling load. The assumption was that the skier, with a mass of 90 $kg$, begins the descent with an initial speed of $2\,m/s$ and accelerates with a constant acceleration of $3.5\,m/s^2$ and $1.5\,m/s^2$ in the linear branch and curved part, respectively.
The Figure 1.39 refers to the spatial displacement on the point B as the ski jumper passes over the ramp. The behaviour is coherent with the presence of a spring in that point, as it counteracts the load, ensuring an (almost) stable structure. The graph indeed shows a vibrating behaviour that then is able to restore its original configuration.

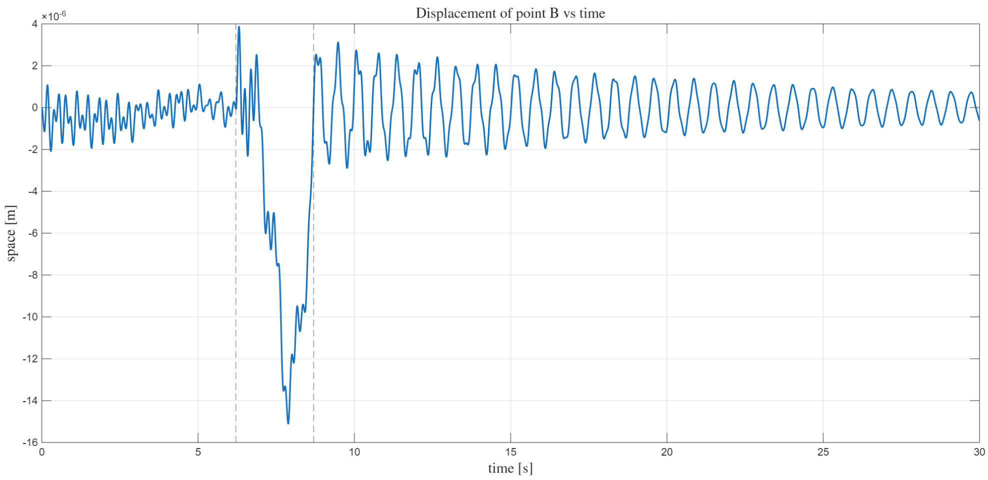


Figure 1.39: Displacement of point B as the moving load passes over the sliding track.

One important thing which can be evidenced is that the highest displacement occurs a bit before the time instant in which the skier reaches the point B. This is given by the fact that the presence of the spring brings the system to be less displaced when the skier is on that point. We tried, in order to prove it, to plot the same graph without considering the concentrated spring, and in that case it is possible to see that the highest displacement actually occurs when the skier in on point B.

In order to obtain this plot, we defined the displacement and the velocity of the skier in function of time. This allowed us to determine which was the distance between the left and right extreme of the finite element with respect to the skier on each time instant.

As we have been able to obtain this information, we applied the given formulas needed to obtain the forces and the moments for each time instant for each node which was influenced. The applied formulas were the following:

The vertical reaction force at node 1:

$$f_{1y}^{(i)} = f_y \left( \frac{a_i b_i (b_i - a_i)}{L_i^3} + \frac{b_i}{L_i} \right) \tag{1.24}$$

The vertical reaction force at node 2:

$$f_{2y}^{(i)} = f_y \left( \frac{a_i b_i (a_i - b_i)}{L_i^3} + \frac{a_i}{L_i} \right) \tag{1.25}$$

The horizontal reaction force at node 1:

$$f_{1x}^{(i)} = f_x \left( \frac{L_i - a_i}{L_i} \right) \tag{1.26}$$

The horizontal reaction force at node 2:

$$f_{2x}^{(i)} = f_x \left( \frac{a_i}{L_i} \right) \tag{1.27}$$

The fixed-end moment at node 1:

$$m_1^{(i)} = f_y \, \frac{a_i b_i^2}{L_i^2} \tag{1.28}$$

The fixed-end moment at node 2:

$$m_2^{(i)} = -f_y \, \frac{b_i a_i^2}{L_i^2} \tag{1.29}$$

Afterwards, we pass from local to global coordinates by using the rotation matrix. As we pass to global coordinates, we create the matrix containing the forces in order to compute the Lagrangian components. Passing to modal approach, it is now necessary to solve:

$$\mathbf{M}_m \, \ddot{\mathbf{q}}(t) + \mathbf{C}_m \, \dot{\mathbf{q}}(t) + \mathbf{K}_m \, \mathbf{q}(t) = \mathbf{Q}_m(t) \tag{1.30}$$

In the state form it is:

$$\frac{d}{dt} \begin{bmatrix} \mathbf{q}(t) \\ \dot{\mathbf{q}}(t) \end{bmatrix} = \begin{bmatrix} \dot{\mathbf{q}}(t) \\ \mathbf{M}_m^{-1} \left[ \mathbf{Q}_m(t) - \mathbf{C}_m \, \dot{\mathbf{q}}(t) - \mathbf{K}_m \, \mathbf{q}(t) \right] \end{bmatrix} . \tag{1.31}$$

It can now be solved by using the MATLAB function `ode45`.

As we solve it and obtain 4 different solutions, we can define the behavior of the 4 modal coordinates in function of time. The result provides us the modal coordinates over time:

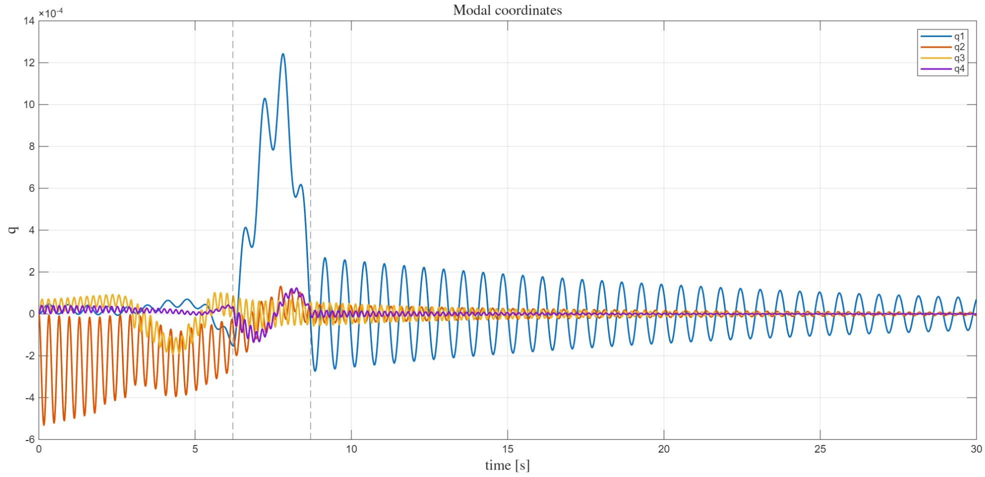


Figure 1.40: Modal coordinates over time.

Recalling that the modal coordinates provide the temporal behavior of the mode-shapes, combining this result with the associated mode-shapes and the sliding of the skier over the structure, the result is aligned with the expected structure movement.

# Final remarks

As engineering students, we particularly appreciate to start applying our mathematical and physical background to solve real and complex engineering systems, and, as a result, this report is interested in highlighting how and, most importantly, why we obtained certain results. This work is the direct outcome of a group which invested on collaboration and commitment.